

High power-added-efficiency AlGaN/GaN HEMTs fabricated by atomic level controlled etching

Xinchuang Zhang(张新创), Bin Hou(侯斌), Fuchun Jia(贾富春), Hao Lu(芦浩), Xuerui Niu(牛雪锐), Mei Wu(武玫), Meng Zhang(张濛), Jiale Du(杜佳乐), Ling Yang(杨凌), Xiaohua Ma(马晓华), and Yue Hao(郝跃)
Citation: Chin. Phys. B, 2022, 31 (**2**): 027301. DOI: 10.1088/1674-1056/ac1414
Journal homepage: http://cpb.iphy.ac.cn; http://iopscience.iop.org/cpb

What follows is a list of articles you may be interested in

Protection of isolated and active regions in AlGaN/GaN HEMTs using selective laser annealing

Mingchen Hou(侯明辰), Gang Xie(谢刚), Qing Guo(郭清), and Kuang Sheng(盛况)
Chin. Phys. B, 2021, 30 (**9**): 097302. DOI: 10.1088/1674-1056/abf34c

Negative transconductance effect in p-GaN gate AlGaN/GaN HEMTs by traps in unintentionally doped GaN buffer layer

Mei Ge(葛梅), Qing Cai(蔡青), Bao-Hua Zhang(张保花), Dun-Jun Chen(陈敦军), Li-Qun Hu(胡立群), Jun-Jun Xue(薛俊俊), Hai Lu(陆海), Rong Zhang(张荣), You-Dou Zheng(郑有炓)
Chin. Phys. B, 2019, 28 (**10**): 107301. DOI: 10.1088/1674-1056/ab3e00

Theoretical analytic model for RESURF AlGaN/GaN HEMTs

Hao Wu(吴浩), Bao-Xing Duan(段宝兴), Luo-Yun Yang(杨珞云), Yin-Tang Yang(杨银堂)
Chin. Phys. B, 2019, 28 (**2**): 027302. DOI: 10.1088/1674-1056/28/2/027302

Transport mechanism of reverse surface leakage current in AlGaN/GaN high-electron mobility transistor with SiN passivation

Zheng Xue-Feng, Fan Shuang, Chen Yong-He, Kang Di, Zhang Jian-Kun, Wang Chong, Mo Jiang-Hui, Li Liang, Ma Xiao-Hua, Zhang Jin-Cheng, Hao Yue
Chin. Phys. B, 2015, 24 (**2**): 027302. DOI: 10.1088/1674-1056/24/2/027302

Degradation mechanism of enhancement-mode AlGaN/GaN HEMTs using fluorine ion implantation under the on-state gate overdrive stress

Sun Wei-Wei, Zheng Xue-Feng, Fan Shuang, Wang Chong, Du Ming, Zhang Kai, Chen Wei-Wei, Cao Yan-Rong, Mao Wei, Ma Xiao-Hua, Zhang Jin-Cheng, Hao Yue
Chin. Phys. B, 2015, 24 (**1**): 017303. DOI: 10.1088/1674-1056/24/1/017303

High power-added-efficiency AlGaN/GaN HEMTs fabricated by atomic level controlled etching

Xinchuang Zhang(张新创)[1], Bin Hou(侯斌)[2], Fuchun Jia(贾富春)[2], Hao Lu(芦浩)[2], Xuerui Niu(牛雪锐)[2], Mei Wu(武玫)[2], Meng Zhang(张濛)[2], Jiale Du(杜佳乐)[2], Ling Yang(杨凌)[2], Xiaohua Ma(马晓华)[2,†], and Yue Hao(郝跃)[2]

[1] *School of Advanced Materials and Nanotechnology, Xidian University, Xi'an 710071, China*
[2] *School of Microelectronics, Xidian University, Xi'an 710071, China*

(Received 7 May 2021; revised manuscript received 23 June 2021; accepted manuscript online 14 July 2021)

An atomic-level controlled etching (ACE) technology is invstigated for the fabrication of recessed gate AlGaN/GaN high-electron-mobility transistors (HEMTs) with high power added efficiency. We compare the recessed gate HEMTs with conventional etching (CE) based chlorine, Cl_2-only ACE and BCl_3/Cl_2 ACE, respectively. The mixed radicals of BCl_3/Cl_2 were used as the active reactants in the step of chemical modification. For ensuring precise and controllable etching depth and low etching damage, the kinetic energy of argon ions was accurately controlled. These argon ions were used precisely to remove the chemical modified surface atomic layer. Compared to the HEMTs with CE, the characteristics of devices fabricated by ACE are significantly improved, which benefits from significant reduction of etching damage. For BCl_3/Cl_2 ACE recessed HEMTs, the load pull test at 17 GHz shows a high power added efficiency (PAE) of 59.8% with an output power density of 1.6 W/mm at $V_d = 10$ V, and a peak PAE of 44.8% with an output power density of 3.2 W/mm at $V_d = 20$ V in a continuous-wave mode.

Keywords: AlGaN/GaN HEMTs, recess etching, low damage, high power added efficiency

PACS: 73.40.Kp, 81.05.Ea, 85.30.De, 85.30.Tv **DOI:** 10.1088/1674-1056/ac1414

1. Introduction

As an excellent representative of third-generation semiconductors, GaN HEMT heterojunction is widely used in high frequency, high efficiency and high power fields, attributing to its high electron mobility (~ 2000 cm^2/V·s), high density (10^{13} cm^{-2}) and high critical breakdown electric field.[1–5] The fabrication of a large number of GaN power electronic devices and RF power devices strongly depends on the etching process.[6–9] However, conventional etching (CE) based on plasma, such as reactive ion etching (RIE) and inductively coupled plasma (ICP), often suffers from some prickly problems including large significant etching damage and uncontrollable etching depth.[10,11] To solve the above problem, atomic layer etching (ALE) of GaN based on XeF_2/BCl_3 and Cl_2/Ar has been proposed.[12,13] Nevertheless, Ohba *et al.* found that an ultrasmooth surface could be realized by ALE based on BCl_3/Cl_2, while ALE based on chlorine-only could result in a rough surface morphology.[14] Kim *et al.* found that when BCl_3 is added to Cl_2, the density of Cl^+ and Cl_2^+ could be significantly reduced during the gas was glow. The decrease of Cl^+ and Cl_2^+ density can significantly reduce the plasma damage.[15] This shows that ALE based on BCl_3/Cl_2 is more potential than ALE of chlorine-only. However, Ohba *et al.* only studied the etching process of AlGaN.[14] Reports on GaN radio frequency devices fabricated by BCl_3/Cl_2 based ALE are still lacking.

In this work, we developed a BCl_3/Cl_2 and Cl_2-only based atomic level controlled etching (ACE) technology for AlGaN. By BCl_3/Cl_2 and Cl_2-only based ACE technology, we fabricated recessed gate HEMTs devices and compared them with HEMTs fabricated by CE process. For the recessed HEMTs with Cl_2-only ACE and BCl_3/Cl_2 ACE technology, the I_{on}/I_{off} ratios of the device are increased by one order of magnitude and more than two orders of magnitude, respectively. At the same time, the DC peak transconductance is increased from 375 mS/mm to 453 mS/mm and 540 mS/mm. At 17 GHz, the HEMTs with Cl_2-only ACE and BCl_3/Cl_2 ACE, respectively, exhibit attractive peak power added efficiency (PAE) of 57.1% and 59.8% at drain bias of 10 V in a continuous-wave mode. The results presented here are believed to boost the low damage etching process for radio frequency applications.

2. Process mechanism of ACE technology

As shown in Fig. 1, the basic BCl_3/Cl_2 ACE concept consists of chemical modification and physical removal. BCl_3/Cl_2-based chemistry is used in ACE for GaN. BCl_3/Cl_2-based free radicals remove residual oxygen and chemically modify the surface atoms of AlGaN, which improve chlorination coverage.[16–18] In the physical reaction step, the kinetic energy of argon ion is precisely controlled by a pulse-

†Corresponding author. E-mail: xhma@xidian.edu.cn

© 2022 Chinese Physical Society and IOP Publishing Ltd

time-regulated RF power, sequentially the chlorine atom layer is just removed.[19–21] A chlorinated layer is formed by the self-limiting chemical reaction between an atomic layer on the GaN surface and the mixed radicals of BCl_3/Cl_2 in Fig. 1 (step 1), ionized by an ICP coil power with the radio frequency of 13.56 MHz. After purging the surplus radicals, the chlorinated layer is removed by argon ions in Fig. 2 (step 2), followed by purging of by-products with BCl_3/Cl_2. The detailed process parameters are shown in the arrow flow charts. It should be noted that the pulse duty in Fig. 2 (step 2) is 30%.

As shown in Fig. 2(a), the AFM (atomic force microscope) scanning morphologies of the etched area surface of the AlGaN samples with 20, 50, 100, 150 and 200 etching cycles are shown with the surface roughness of 0.221 0.241 0.257 0.259 and 0.313 nm by BCl_3/Cl_2 ACE, and the corresponding etching depths are 11, 26, 52, 78 and 105 nm, respectively. The root-mean-square (RMS) roughness of initial un-etching sample is 0.253 nm. With the increase of the number of ACE cycles, the etching depth increases linearly, and the surface roughness of the etched area remains constant at a very low level. The etch per cycle (EPC) is 0.52 nm/cycle, which is in agreement with the lattice constant of GaN along c axis.[22] Although the numbers of ACE cycles for all the samples are different, their EPCs are the same, which indicates that the ACE technology has excellent repeatability and stability. What's more, BCl_3/Cl_2 ACE is capable of realizing atomic-scale control of AlGaN. The EPC of Cl_2-only ACE is 0.54 nm/cycle which is slightly larger than the ones of BCl_3/Cl_2 ACE. This may be due to the plasma damage caused by more Cl^+ and Cl_2^+ in the chlorine plasma. By adding BCl_3 into Cl_2, the concentration of Cl^+ and Cl_2^+ is reduced and the plasma damage is suppressed in the step of chemical modification.[15] Figure 2(b) compares between chemical modification only, physical removal only, and the EPC of BCl_3/Cl_2 ACE (full cycle). The two key steps (in Fig. 1 step 1 and step 2) are executed separately for 200 cycles. The EPC of chemical modification is zero, while ones of physical removal is 0.07 nm/cycle. This indicates that the chemical modification and physical removal of BCl_3/Cl_2 ACE are completely separated in time. However, the EPC of chemical modification only and the ones of physical removal only for Cl_2-only ACE are 0.02 and 0.07 nm/cycle. This result shows that there is a slight etching effect in the chlorine glow process.

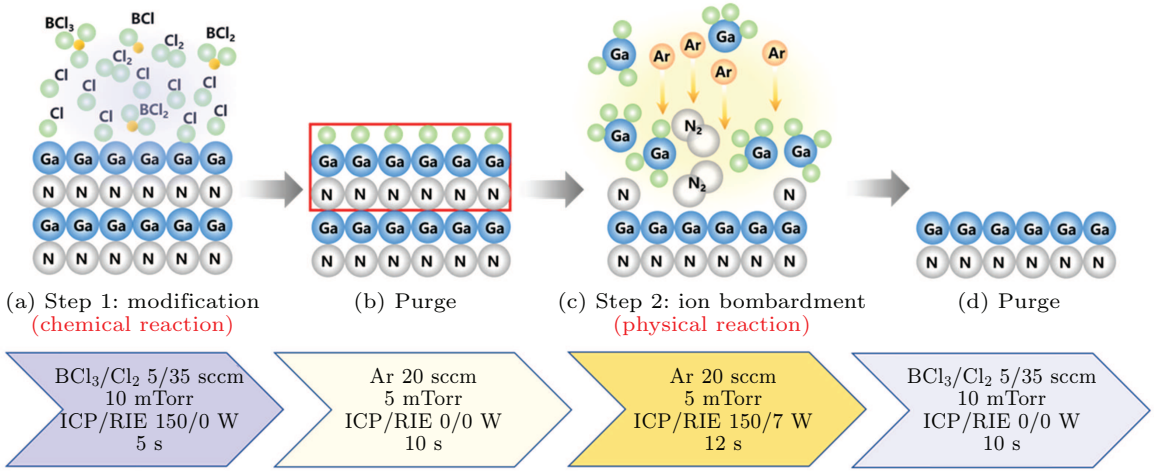


Fig. 1. ACE cyclic process: (a) chlorination of GaN surface atomic layer by BCl_3/Cl_2 radicals; (b) pump out the excessive free radicals and purge chamber with Ar; (c) argon ion bombards the chlorinated atomic layer to form; (d) pump out the by-products and purge chamber with BCl_3/Cl_2.

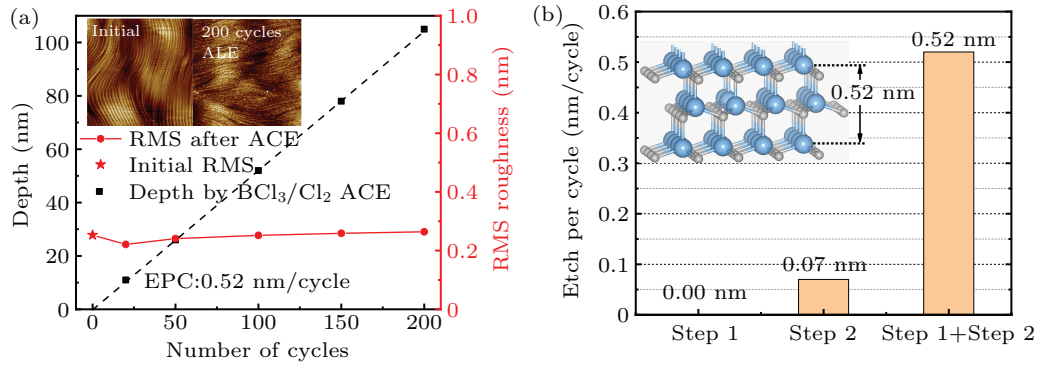


Fig. 2. (a) Etching depth and RMS roughness versus the number of BCl_3/Cl_2 ACE cycles (inset: surface topography (area: 5 μm × 5 μm) of the initial unetched sample and the sample with 200 cycles ACE). (b) Result of EPC test based on BCl_3/Cl_2.

3. Device structure and fabrication

As shown in Fig. 3(a), the AlGaN/GaN HEMT fabricated in this work was grown on a 3-inch SiC substrate, which comprises a 3-nm GaN cap layer, a 21-nm $Al_{0.25}Ga_{0.75}N$ barrier layer, a 400-nm i-GaN channel, and a GaN buffer layer from top to bottom. An electron sheet concentration of 8.29×10^{12} cm^{-2}, a sheet resistance of 303 Ω/□, and a mobility of 1946 cm^2/V·s were measured by room-temperature Hall measurements. The ohmic contact formation of source and drain included a deposition of Ti/Al/Ni/Au metal stack and annealed at 840 °C for 30 s in N_2. Nitrogen ion implantation was then used for device isolation. Transfer length method (TLM) showed an ohmic contact resistance of 0.39 Ω·mm. A 60-nm plasma enhanced chemical vapor deposition (PECVD) SiN_x was utilized as a passivation layer. Electron beam lithography defined the recessed-gate foot of 0.17 μm. After CF_4 based plasma removing the passivation layer, the AlGaN barrier layer was recessed by BCl_3/Cl_2 ACE and Cl_2-only ACE technology. The recessed depth was measured to be 18 nm by AFM with 35 and 33 cycles, resulting in an EPC of 0.52 and 0.54 nm/cycle, respectively. For comparison, 18 nm recess was etched by CE process (the rate of CE is 3 nm/min with an ICP coil power of 150 W, a bias power of 5 W, operating pressure of 5 mTorr, BCl_3/Cl_2 (20 sccm/20 sccm), process time of 6 min), the depth of which was controlled by the process time. Figures 3(b), 3(c) and 3(d) illustrate the AFM surface morphology of the sample with CE, Cl_2-only ACE and BCl_3/Cl_2 based ACE recessed etching process, respectively. It is shown that the surface morphology maintains a clear and continuous atomic step and a very low surface roughness with RMS roughness of 0.220 nm after BCl_3/Cl_2 based ACE. The Cl_2-only ACE-HEMT shows a rough surface morphology with RMS roughness of 0.257 nm, while the recessed gate with CE shows a roughness of 0.353 nm. After the gate lithography, the Ni/Au/Ni gate metal was deposited. The gate root width (L_g), gate head width, source-drain spacing (L_{sd}), and source-gate space (L_{sg}) are 0.17 μm, 0.9 μm, 2.5 μm, and 1 μm, respectively.

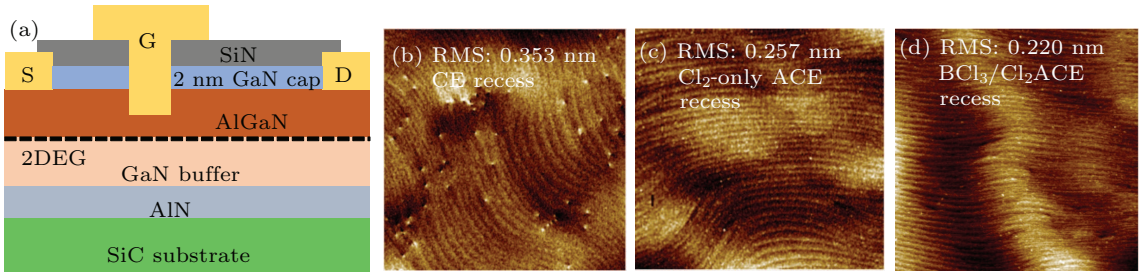


Fig. 3. (a) Schematic diagram of recessed AlGaN/GaN HEMTs, and surface topography (area: 5 μm ×5 μm) of (b) CE recess, (c) Cl_2-only ACE recess, and (d) BCl_3/Cl_2 ACE recess.

4. Results and discussion

The DC transfer I_d–V_g, output I_d–V_d, gate reverse Schottky characteristics and the field-effect mobility (μ_{FE}) with gate voltage of the recessed gate HEMTs by the CE, Cl_2-only ACE and BCl_3/Cl_2 ACE process are performed. As shown in Fig. 4(a), owing to precise controlling bombardment and effectively suppressed etching damage of the ACE technology, the drain leakage current of the device decreases from 2.7×10^{-5} to 3.7×10^{-6} and 2.6×10^{-7} A/mm, the I_{on}/I_{off} ratio increases from 4.9×10^4 to 4.8×10^5 and 6.8×10^6, and the peak transconductance of the device increased from 375 to 453 and 540 mS/mm. Figure 4(b) shows that the drain saturation current was raised from 785 to 995 and 1031 mA/mm for three types of HEMTs. As can be seen from Fig. 4(c), compared with the HEMTs by the CE, the gate leakage of HEMTs by Cl_2-only ACE and HEMTs by BCl_3/Cl_2 ACE decreases by one order of magnitude and more than two orders of magnitude respectively. Figure 4(d) shows the transfer I–V sweep in linear region and extracted μ_{FE} as a function of V_g. The μ_{FE} of the recessed-HEMTs channel was studied with L_{sg}, L_g, L_{gd} and L_{sd} of 3, 50, 3 and 56 μm devices, in which the influence of series resistance on Gm was negligible. The peak mobility of recessed HEMT with the Cl_2-only ACE and BCl_3/Cl_2 ACE process is 1204 and 1487 cm^2/V·s. However, ones of the HEMT with CE is 953 cm^2/V·s. It was probably due to the fact that ACE did not cause the loss of nitrogen in the process of recessing the AlGaN barrier and ultimately reduced the surface trap concentration.[23] The peak mobility of recessed HEMT with the Cl_2-only ACE is lower than that of recessed HEMT with BCl_3/Cl_2ACE, which may be caused by plasma damage during chlorination (Fig. 1, step 1).

Figure 5 shows the pulse transfer characteristics of three types of HEMTs at a gate voltage of −6 V to 2 V and the current collapse ratio can be expressed as

$$\Delta I = \Delta I_{ds}/I_{ds0}, \tag{1}$$

where ΔI_{ds} is the variation of drain pulse current ($V_g = 2$ V) before and after electrical stress, and I_{ds0} is the drain pulse current ($V_g = 2$ V) before applying electric stress.

The HEMTs with Cl_2-only ACE and BCl_3/Cl_2 ACE show current collapse (collapse ratio: 4.1%, Fig. 5(b); 2.7%, Fig. 5(c)), under a quiescent bias of $(V_{GSQ}, V_{DSQ}) = (-8$ V, 0 V). They are all smaller than a value of 6.3% for CE

HEMTs. At (V_{GSQ}, V_{DSQ}) = (−8 V, 20 V), the current collapse ratio decreases from 25.2% (CE HEMT) to 13.1% (Cl_2-only ACE) and 8.5% (BCl_3/Cl_2 ACE). The BCl_3/Cl_2 ACE HEMT and Cl_2-only ACE HEMT show tiny threshold voltage shift (ΔV_{th} = 0.04 V and 0.14 V) under a quiescent bias of (V_{GSQ}, V_{DSQ}) = (−8 V, 20 V), while that of CE ones is 0.28 V. Such shift may be caused by the trapped electrons introduced under the gate during the recessing process.[23]

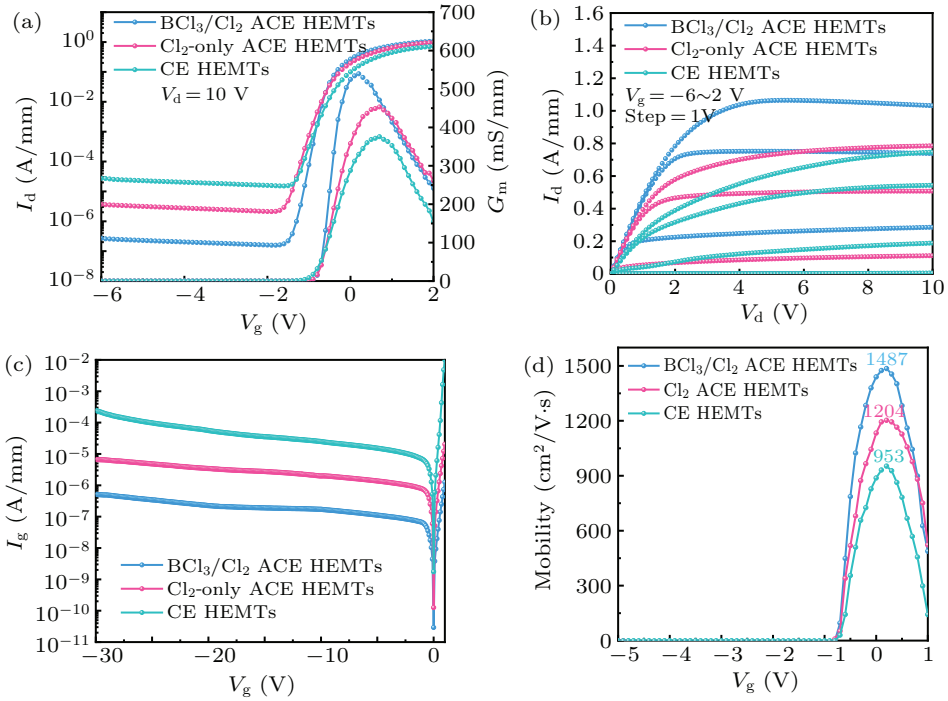


Fig. 4. DC characteristics of the recessed AlGaN/GaN HEMTs with ACE and CE gate recess. (a) Transfer characteristics at V_d = 10 V, (b) output characteristics, (c) gate reverse leakage characteristics, (d) field-effect mobility as a function of gate voltage for three types of HEMTs.

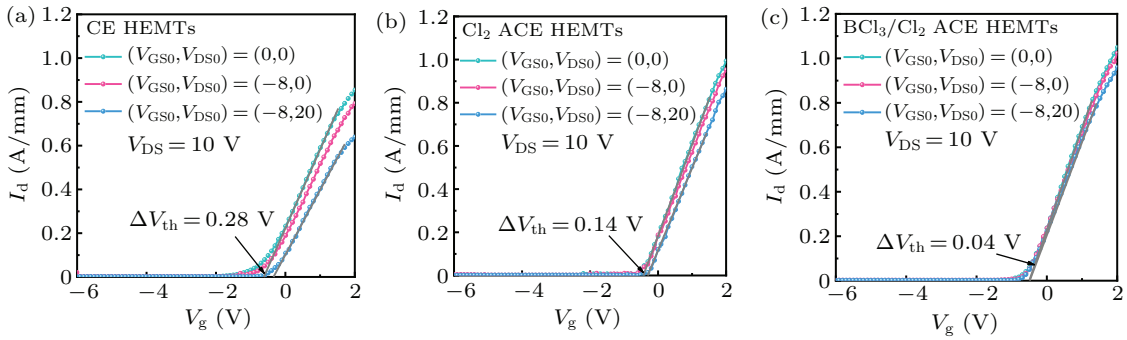


Fig. 5. Pulsed transfer *I*–*V* characteristics of recessed gate HEMTs with (a) CE, (b) Cl_2-only ACE , (c) BCl_3/Cl_2 ACE at a gate voltage of −6 V to 2 V for (V_{GSQ}, V_{DSQ} = 0 V, 0 V), (V_{GSQ}, V_{DSQ} = −8 V, 0 V) and (V_{GSQ}, V_{DSQ} = −8 V, 20 V).

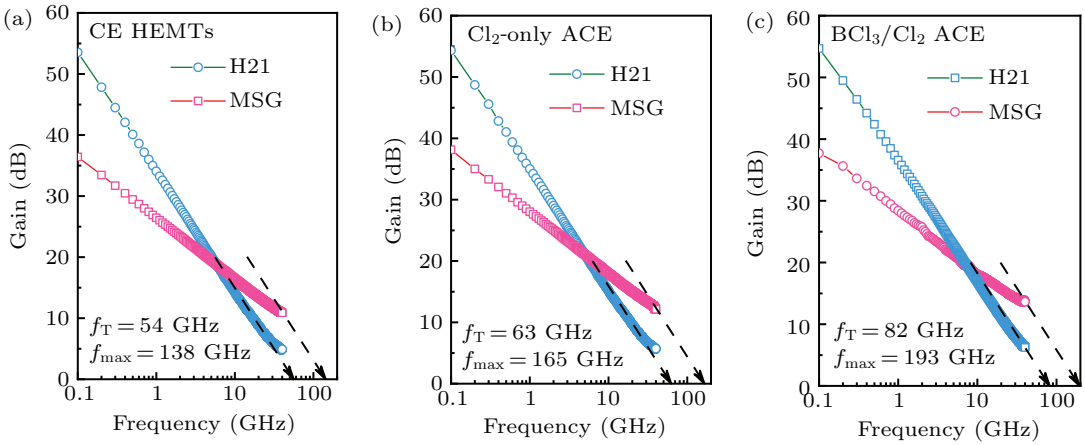


Fig. 6. Small-signal characteristics of the recessed HEMTs at V_d = 10 V, V_g = 0.2 V with (a) CE gate recess and (b) Cl_2-only ACE gate recess, (c) BCl_3/Cl_2 ACE gate recess.

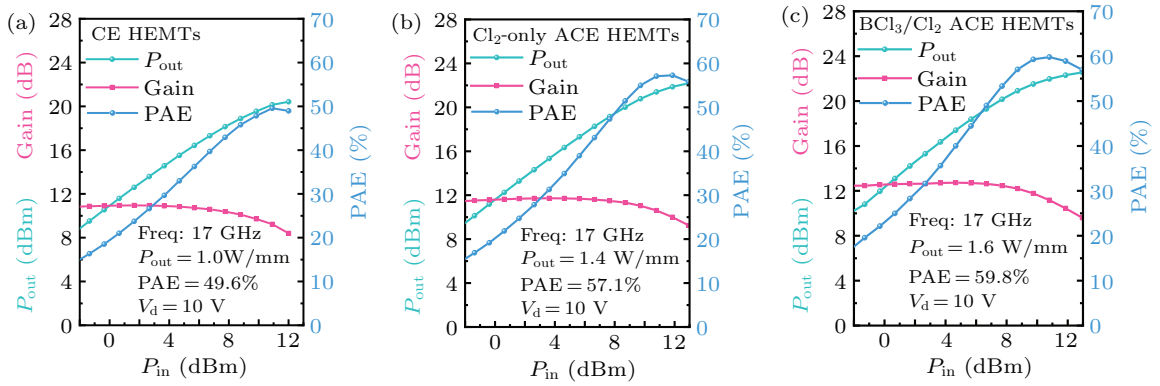


Fig. 7. Load-pull characteristics of the fabricated HEMTs at 17 GHz with $W_G = 2 \times 50$ μm in CW mode. (a) CE recessed, (b) Cl_2-only ACE recessed, and (c) BCl_3/Cl_2 ACE recessed.

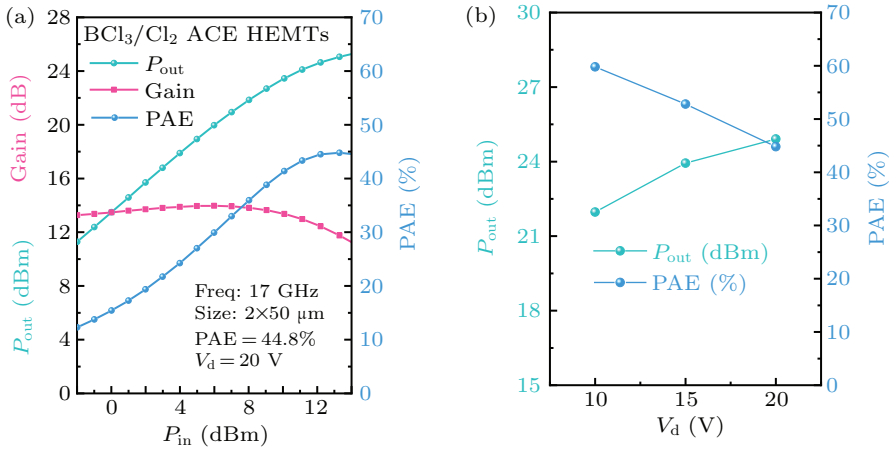


Fig. 8. Large-signal characteristics of BCl_3/Cl_2 ACE HEMTs at 17 GHz with $W_G = 2 \times 50$ μm in CW mode: (a) at $V_d = 20$ V, (b) RF output power density and peak PAE versus V_d.

Small-signal measurements was used to compare the current-gain cutoff frequency (f_T) and maximum oscillation frequency (f_{max}) of the three kinds of recessed gate HEMTs in the frequency range from 0.1 GHz to 40 GHz. As shown in Figs. 6(b) and 6(c), under the same bias condition of $V_d = 10$ V and $V_g = 0.2$ V, the BCl_3/Cl_2 ACE-HEMT and Cl_2-only ACE-HEMT show a f_T/f_{max} of 82/193 GHz and 63/165 GHz, respectively. However, the ones of CE-HEMT were 54 and 138 GHz, respectively, as shown in Fig. 6(a). This is consistent with the law of channel field effect mobility.

The large-signal microwave power measurements of recessed HEMTs with ACE and CE were carried out at 17 GHz in continuous-wave (CW) mode, as shown in Fig. 7. All devices were biased at $V_d = 10$ V and class-AB condition. Benefiting from the suppressed gate leakage current as well as the current collapse,[24] the large-signal performance of the recessed HEMTs with ACE has been significantly improved compared with the CE-HEMT, high PAEs of 59.8% and 57.1% are achieved in the BCl_3/Cl_2 ACE-HEMT and Cl_2-only ACE-HEMT, which is about 10.2% and 7.5% higher than those with CE. In addition, the corresponding output power density has also been increased to 1.6 W/mm and 1.4 W/mm, respectively, while that for the CE HEMTs is 1.0 W/mm.

In order to evaluate the higher voltage operation of the BCl_3/Cl_2 ACE-HEMTs, we performed the large-signal test at $V_d = 20$ V biased in a CW mode, as shown in Fig. 8(a). The peak PAE of BCl_3/Cl_2 ACE-HEMTs is 44.8% with the output power density of 3.2 W/mm at 17 GHz. Output power density and peak PAE as a function of drain voltage ($V_d = 10$, 15 and 20 V) for BCl_3/Cl_2 ACE-HEMTs are shown in Fig. 8(b). When $V_d = 15$ V, the output power density is 2.5 W/mm and the peak PAE is 52.8%. With the increase of drain bias voltage, the peak PAE decreases, which may be related to the increase of gate leakage current as shown in Fig. 4(c).[25] The further study will focus on the PAE improvement at higher operation voltage such as using N_2O plasma treatment.[26]

5. Conclusion and perspectives

An atomic level controlled etching technology is proposed for fabrication of recessed gate AlGaN/GaN HEMTs. Adding BCl_3 to the chlorination process significantly reduces the roughness of the AlGaN etched surface. The etching depth of the AlGaN can be controlled accurately due to precise power control. The BCl_3/Cl_2 ACE-recessed AlGaN/GaN HEMTs exhibits an attractive PAE of 59.8% at 17 GHz in a CW mode. The ACE technology can solve the current prob-

lem of conventional plasma etching in the fabrication of recessed AlGaN/GaN devices, and AlGaN/GaN Fin-FET devices, which is full of potential in the future development of GaN technology.

Acknowledgements

This work was supported by the National Natural Science Foundation of China (Grant Nos. 62090014, 62188102, 62104184, 62104178, and 62104179) and the Fundamental Research Funds for the Central Universities of China (Grant Nos. XJS201102, XJS211101, XJS211106, and ZDRC2002).

References

[1] Chung J W, Hoke W E, Chumbes E M and Palacios T 2010 *IEEE Electron Dev. Lett.* **31** 195
[2] Hao Y, Yang L, Ma X H, Ma J G, Cao M Y, Pan C Y, Wang C and Zhang J C 2011 *IEEE Electron Dev. Lett.* **32** 626
[3] Wu Y F, Saxler A, Moore M, Smith R P, Sheppard S, Chavarkar P M, Wisleder T, Mishra U K and Parikh P 2004 *IEEE Electron Dev. Lett.* **25** 117
[4] Ma J, Zhu M and Matioli E 2017 *IEEE Electron Dev. Lett.* **38** 1704
[5] Rüdiger Q 2008 *Gallium Nitride Electronics* (Berlin: Springer-Verlag) Vol. 96 pp. 19–21
[6] Wang H, Xie R, Liu C, Wei J, Tang G and Chen K J 2016 *IEEE Energy Conversion Congress and Exposition (ECCE)*, September 18–22, 2016, Milwaukee, WI, USA, pp. 1–6
[7] Li X, Hove M V, Zhao M, Geens K, Lempinen VP, Sormunen J, Groeseneken G and Decoutere S 2017 *IEEE Electron Dev. Lett.* **38** 918
[8] Zhang K, Kong Y, Zhu G, Zhou J, Yu X, Kong C, Li Z and Chen T 2017 *IEEE Electron Dev. Lett.* **38** 615
[9] Marti D, Tirelli S, Alt A R, Roberts J and Bolognesi C R 2012 *IEEE Electron Dev. Lett.* **33** 1372
[10] Shul RJ, Zhang L, Baca AG, Willison CG, Han J, Pearton SJ, Lee KP and Ren F 2001 *Solid State Electron.* **45** 13
[11] Cao X A, Cho H, Pearton S J, Dang G T, Zhang A P, Ren F, Shul R J, Zhang L, Hickman R and Van Hove J M 1999 *Appl. Phys. Lett.* **75** 232
[12] Johnson N R, Hite J K, Mastro M A, Jr C R Eddy and George S M 2019 *Appl. Phys. Lett.* **114** 243103
[13] Kauppinen C, Khan S A, Sundqvist J, Suyatin D B, Suihkonen S, Kauppinen E I and Sopanen M 2017 *J. Vac. Sci. Technol. A* **35** 060603
[14] Ohba T, Yang W, Tan S, Kanarik K J and Nojiri K 2017 *Jpn. J. Appl. Phys.* **56** 06HB06
[15] Kim H S, Lee D H, Lee J W, Kim T I and Yeom G Y 2000 *Vacuum* **56** 45
[16] Wu T, Hao Z, Tang G and Luo Y 2003 *Jpn. J. Appl. Phys.* **42** L257
[17] Kanarik K J *et al.* 2017 *J. Vac. Sci. Technol. A* **35** 05C302
[18] Zhirnov E, Stepanov S, Wang W N, Shreter Y G, Takhin D V and Bochkareva N I 2004 *J. Vac. Sci. Technol. A* **22** 2336
[19] Samukawa S and Terada K 1994 *Proceedings of VLSI Technology Symposium*, June 7–9, 1994 Honolulu, HI, USA, p. 27
[20] Ohtake H, Samukawa S, Noguchi K, Lida H Sato A and Qian X 1999 *Plasma Process-Induced Damage, 1999 4th International Symposium on Plasma Process-Induced Damage*, May 9–11, 1999, Monterey, CA, USA, p. 37
[21] Kumagai S, Shiraiwa T and Samukawa S 2004 *J. Vac. Sci. Technol. A* **22** 1093
[22] Mohammad S N and Morko H 1996 *Prog. Quantum Electron.* **20** 361
[23] Wang X, Huang S, Zheng Y, Wei K, Chen X, Zhang H and Liu X 2014 *IEEE Trans. Electron Devices* **61** 1341
[24] Zhang Y, Huang S, Wei K, Zhang S Wang X, Zheng Y, Liu G, Chen X, Li Y and Liu X 2020 *IEEE Electron Dev. Lett.* **41** 701
[25] Jimenez J L and Chowdhury U 2008 *IEEE International Reliability Physics Symposium*, April 27–May 1, 2008, Phoenix, AZ, USA p. 429
[26] Mi M H, Ma X H, Yang L, Lu Y, Hou B, Zhu J J, Zhang M, Zhang H S, Zhu Q, Yang L A and Hao Y 2017 *IEEE Trans. Electron Devices* **64** 4875